General Disclaimer

One or more of the Following Statements may affect this Document

- This document has been reproduced from the best copy furnished by the organizational source. It is being released in the interest of making available as much information as possible.

- This document may contain data, which exceeds the sheet parameters. It was furnished in this condition by the organizational source and is the best copy available.

- This document may contain tone-on-tone or color graphs, charts and/or pictures, which have been reproduced in black and white.

- This document is paginated as submitted by the original source.

- Portions of this document are not fully legible due to the historical nature of some of the material. However, it is the best reproduction available from the original submission.

NASA TECHNICAL MEMORANDUM

NASA TM X-71842

NASA TM X-71842

ANALYSIS OF RADIALLY CRACKED RING SEGMENTS SUBJECT TO FORCES AND COUPLES

by Bernard Gross and John E. Srawley
Lewis Research Center
Cleveland, Ohio 44135

TECHNICAL PAPER to be presented at Committee E-24 Symposium on Developments in Fracture Mechanics Tests sponsored by the American Society for Testing and Materials
St. Louis, Missouri, May 2-7, 1976

ANALYSIS OF RADIALLY CRACKED RING SEGMENTS SUBJECT TO FORCES AND COUPLES

by Bernard Gross and John E. Srawley

National Aeronautics and Space Administration
Lewis Research Center
Cleveland, Ohio 44135

ABSTRACT

Results of planar boundary collocation analysis are given for ring segment (C shaped) specimens with radial cracks, subjected to combined forces and couples. Mode I stress intensity factors and crack mouth opening displacements were determined for ratios of outer to inner radius in the range 1.1 to 2.5 and ratios of crack length to segment width in the range 0.1 to 0.8.

E-8567

INTRODUCTION

The ASTM E399 Standard Method of Test for Plane-Strain Fracture Toughness of Metallic Materials is presently confined to two types of specimens, namely: bend or compact (ref. 1). It can be both expensive and wastefull of material to fabricate such standard specimens from tubes. For this reason, Kendall et al (refs. 2 to 5) have proposed a new type of standard specimen, namely a ring segment (commonly called C shaped) specimen which contains a radial crack.

The ASTM E-24 Committee on Fracture Testing of Metals is currently considering this type of specimen as a possible standard. Stress intensity factors for such specimens were obtained by Kendall et al (refs. 2 to 5) by a boundary collocation technique in which a large number of boundary stations (up to 250) was employed in conjunction with an overdetermined system of equations. They obtained stress intensity factors for ring segments with internal radial cracks loaded by opposed tensile forces with a

line of action along a chord normal to the crack. The stress distribution produced by this manner of loading is due largely to the bending moment about mid net section; the resultant normal force has only a minor effect.

To augment and compare with the results of refs. 2 to 5, we undertook an independent analysis in which by use of a different application of boundary conditions, the number of boundary points was greatly reduced. The solution obtained herein provides results for any combination of bending moment and normal force acting on a ring segment with a radial crack on either the inner or outer surface.

Consider either of the specimens shown in figs. 1(a) and 1(b), internally cracked and subjected to tensile forces P normal to the crack, or externally cracked and subjected to normal compressive forces. One practical method of loading is through pins acting on the surfaces of holes in the specimens as shown. The line of action of the load is at a distance x from the intersection of a line drawn along the crackline with the inner radius R_i. The ratio x/W, where W is the wall thickness is one of the independent parameters in this study. The other independent parameters are the relative crack length a/W, and the radius ratio of the ring $R_o/R_i = 1 + W/R_i$.

The present treatment of such specimens follows that of a companion paper on the rectangular side cracked specimens, ref. 6, in that the loading of the specimen is characterized by the statically equivalent combination of resultant force P, chosen to act through mid net section, and complementary couple, of moment M, as shown in fig. 1(a) and (b). The advantage of this approach is that the stress intensity coefficient Γ or crack mouth opening coefficient Δ for any value of x/W can be obtained

efficiently by superposition of two complementary special cases, namely net section tension where the value of moment of the complementary couple is zero, and net section bending where the value of the normal force is zero. The superposition of these two complementary cases involves only interpolation, not extrapolation.

In applying the boundary collocation analysis the specimens of figs. 1(a) and (b) are modeled by the ring half segments as shown in figs. 1(c) and (d), where the angle θ is a variable of the analysis. The boundary conditions along B C are obtained from the known solution for the stress distribution in an uncracked half ring subject to a combination of force and couple, ref. 7. For the special case of net section tension (M = 0) the moment of the counter couple acting on the half ring boundary is such that it balances the moment of the force about the midpoint of the net section. For the special case of net section bending (P = 0), the value of the force is zero. By combining these two special solutions, the solution can be obtained for any load P of figs. 1(a) and (b), as shown in fig. 2. Boundary collocation analyses were conducted for increasing values of the angle θ up to an angle θ_o, beyond which no significant change in the values of the stress intensity factor, or the crack mouth displacement occurred. The results presented here will therefore apply to those practical specimens for which the loading forces are sufficiently removed such that the stress distribution of an uncracked ring at the boundary with angle θ_o corresponds closely to that employed here.

SYMBOLS

a crack length

B specimen depth

E young modulus

$E' = E/(1 - \nu^2)$	for plane strain conditions
$E' = E$	for plane stress conditions
K_I	mode I stress intentisy factor
M	applied end couple
$\bar{n}$	unit outward normal vector along all boundaries
P	applied end force
R_i	ring segment inner radius
R_o	ring segment outer radius
r, θ	polar coordinate system
v	total crack mouth opening
W	curved beam wall thickness, $(R_o - R_i)$
$\Gamma = \frac{K_I}{(\sigma_P + \sigma_M)\sqrt{a(1 - a/W)}}$	stress intensity coefficient, a function of three independent variables $(R_o/R_i,\ a/W,\ \omega)$
$\Delta = \frac{E'v}{(\sigma_P + \sigma_M)a}$	crack mouth displacement coefficient, a function of three independent variables $(R_o/R_i,\ a/W,\ \omega)$
θ_o	angle determining the far boundary in the boundary collocation solution
ν	poissons ratio
σ_M	$6M/B(W-a)^2$ component of fictitious normal net stress due to moment M
σ_P	$P/B(W-a)$ component of fictitious normal net stress due to load P
χ	stress function
ω	independent variable, $\arctan(\sigma_M/\sigma_P)$

NUMERICAL RESULTS

Calculations were performed for mode I crack deformation on each of the two cases shown in fig. 2. The stress function boundary conditions appropriate to each case are given in the Appendix. Stress intensity factors and crack mouth displacements were obtained for both internal and external radially cracked ring segments for all combinations of eight a/W ratios from 0.1 to 0.8, with three R_o/R_i ratios: 1.1, 1.5 and 2.5. The results presented herein were obtained using the boundary collocation technique with 60 boundary points and an overdetermined system of equations, as detailed in refs. 8 and 9.

Fig. 3 compares values of the stress intensity coefficient with

$$\Gamma = \frac{K_I}{(\sigma_P + \sigma_M)\sqrt{a(1 - a/W)}} \tag{1}$$

corresponding values from ref. 5.

The stress intensity coefficients, for three types of end load conditions, are listed in tables I, II, and III. Similarly, the crack mouth displacement coefficients are listed in tables IV, V, and VI. The advantages of characterizing the stress intensity factor and mouth displacements respectively as Γ and Δ are discussed in ref. 6. Tables I, II, IV, and V are for superposition use. For example, we are given a curved beam with an internal crack, a/W = 0.5, R_o = 11, and R_i = 10, and boundary load conditions such that at x/W = 0.5 the resultant pin load is P (fig. 2). To find Γ, the values of Γ_P (table I) for a combined end load P and end couple $M_I = P(R_i + (W + a)/2)$ are superimposed with the values of Γ_M (table II) due to end couple $M_{II} = M_I - P(R_i + x)$:

Since $K_{I_{\text{Resultant}}} = K_{I_{\text{Table I}}} + K_{I_{\text{Table II}}}$ by superposition, from eq. 1

we obtain

$$\Gamma = \frac{\Gamma_P \sigma_P + \Gamma_M \sigma_M}{\sigma_P + \sigma_M} \tag{2}$$

Through algebraic manipulation

$$\frac{\sigma_P}{\sigma_P + \sigma_M} = \frac{1 - a/W}{2(a/W + 2 + 3x/W)} = \frac{1}{16}$$

and

$$\frac{\sigma_M}{\sigma_P + \sigma_M} = \frac{3(1 + a/W + 2x/W)}{2(a/W + 2 + 3x/W)} = \frac{15}{16}$$

From tables I and II we have

$$\Gamma_P = 0.711 \quad \text{and} \quad \Gamma_M = 0.943$$

From equation 2 we obtain $\Gamma = 0.926$, which is consistent with the value plotted in fig. 3(a).

RESULTS AND DISCUSSION

Fig. 3 is a comparison of present stress intensity factor results with those from ref. 5. The referenced results were obtained using a large number of boundary stations (up to 250) in conjunction with an overdetermined system of equations. Modifications of the boundary conditions made herein as given in the appendix, enables the use of many fewer stations. With 30 stations the stress intensity factors differed by only about one percent from those obtained with 60 stations. However for more accurate displacement values, 60 boundary points, equally distributed were used.

The specimen as shown in fig. 3 and analyzed in ref. 5 and herein is such that with the load P applied at $x/W = 0.5$, at the mid net section we have bending moment $M = P(2W + a)/2$, so that the ratio $\sigma_M/\sigma_P =$

$3(2W + a)/(W - a)$. Good agreement on comparing the results of ref. 5 and results obtained herein, is found for ratios R_o/R_i of 1.481 and 2.963. However, for $R_o/R_i = 1.212$ the agreement is poor. As a check the results from ref. 6 for the limiting case of a straight bar ($R_o/R_i = 1$) subject to a statically equivalent load and moment are also included in fig. 3. From this it appears that the results obtained herein are consistent with the expected monotonic approach to the limit case as R_o/R_i approaches unity. In contrast the results from ref. 5 are not consistent with this expectation. Tables I through VI contain boundary collocation values of stress intensity factors and displacement respectively in terms of dimensionless coefficients Γ and Δ, which are functions of three independent variables ω, a/W and R_o/R_i.

It will be noted that in table I the values of Γ for external cracks are greater than the corresponding values for internal cracks, whereas in tables II and III the reverse is the case. This circumstance is a consequence of two separate factors which have opposite effects:

(1) The neutral surface in an uncracked curved bar is closer to the inner, concave surface than to the outer convex surface. This feature of the boundary stress distribution enhances the stress intensity factor for an internally cracked ring segment but depresses it when the ring segment is externally cracked, providing that no other factor has a stronger counter effect.

(2) When there is an applied countercouple which balances the moment of the force P about mid net section, the value of the moment is greater for the internally cracked specimen, $P(2R_i + W + a)/2$, than for the externally cracked specimen, $P(2R_i + W - a)/2$. Such a countercouple therefore reduces the stress intensity factor for an internally cracked

segment more than for one which is externally cracked. The results of table I reflect a stronger effect of the second factor than of the first. Those of tables II and III reflect only the effect of the first factor. An analogous explanation holds for the displacement results of tables IV, V, and VI.

Tables III and VI give the values of Γ and Δ which were obtained directly by boundary collocation for ring segments subject to opposed end forces which act along the diameter normal to the crack plane. For this case as a check, superimposing the results shown in tables I and II leads to values which are within one percent of the values in table III.

Fig. 4 is a plot of values of tables I, II, and III for an internal crack with $R_o/R_i = 2.5$. The results shown in table III are numerically close to those shown in table II. Hence for reasonable values of x, the extrapolations necessary using tables II and III can lead to much less accurate values of the resultant stress intensity coefficient Γ than an interpolation between the results given in tables I and II. Thus, tables II and III should not be used in the application of the superposition principle.

The accuracy with which the results presented herein apply depends on the extent to which the assumed boundary conditions approximate the actual boundary conditions. Fig. 5, shows the location of boundary (B) (C) for various R_o/R_i ratios, which is sufficiently distant from the crack plane so as to not be affected by the crack.

APPENDIX

The results presented here were obtained by plane elastostatic boundary collocation analysis of a homogeneous isotropic body. This method of analysis is described in detail by Gross and Mendelson et al. (refs. 8 and 9). The boundary conditions to be satisfied by the stress function and its normal derivative along the boundary were obtained from the known solution for the stress distribution in a half ring subjected to forces and couples (ref. 7). The models analyzed herein are segments of half rings containing radial cracks as shown in figs. A1 and A2. For computational purposes the boundaries were radial cuts defined by the angle θ. This angle is a variable of the analysis which is progressively increased until further increase ($\theta > \theta_o$) produces no significant change in the results.

The boundary conditions for the internally cracked model are as follows:

Figure (A1a)

For the ring segment subject to forces P, with $\theta = \theta_o$, and boundaries AB, BC, CD along arc AB

$$\chi(R_i, \theta) = 0$$

$$\left.\frac{\partial \chi}{\partial n}\right|_{R_i, \theta} = 0$$

along line BC

$$\chi(R, \theta_o) = \frac{-P\cos\theta_o}{\left(R_i^2 - R_o^2\right) + \left(R_i^2 + R_o^2\right)\ln(R_o/R_i)} \times \left[\frac{R^3}{2} - \frac{R_i^2 R_o^2}{2R} - R\left(\left(R_i^2 + R_o^2\right)\ln\frac{R}{R_i} + \left(\frac{R_i^2 - R_o^2}{2}\right)\right)\right]$$

$$\left.\frac{\partial \chi}{\partial n}\right|_{R,\,\theta_o} = \frac{P \sin \theta_o}{\left(R_i^2 - R_o^2\right) + \left(R_i^2 + R_o^2\right) \ln\left(\frac{R_o}{R_i}\right)}$$

$$\times \left[\frac{R^2}{2} - \frac{R_i^2 R_o^2}{2R^2} - \left(R_i^2 + R_o^2\right) \ln \frac{R}{R_i} - \left(\frac{R_i^2 - R_o^2}{2}\right)\right]$$

along arc CD

$$\chi(R_o, \theta) = PR_o \cos \theta$$

$$\left.\frac{\partial \chi}{\partial n}\right|_{R_o,\,\theta} = P \cos \theta$$

Figure (A1b)

For the couple load with $\theta = \theta_o$ and boundaries AB, BC, CD along arc AB

$$\chi(R_i, \theta) = 0$$

$$\left.\frac{\partial \chi}{\partial n}\right|_{R_i,\,\theta} = 0$$

along line BC

$$\chi(R, \theta_o) = \frac{M}{\left(R_o^2 - R_i^2\right)^2 - 4R_o^2 R_i^2 \left(\ln\left(\frac{R_o}{R_i}\right)\right)^2}$$

$$\times \left[-4 R_o^2 R_i^2 \ln \frac{R_o}{R_i} \ln R - 2\left(R_o^2 - R_i^2\right) R^2 \ln R + R^2 \left(R_o^2 - R_i^2\right)\right.$$

$$\left. + 2\left(R_o^2 \ln R_o - R_i^2 \ln R_i\right) R^2 + R_i^2 \left(2R_o^2 \ln \frac{R_o}{R_i}(2 \ln R_i - 1) - \left(R_o^2 - R_i^2\right)\right)\right]$$

$$\left.\frac{\partial \chi}{\partial n}\right|_{R,\,\theta_o} = 0$$

along arc CD

$$\chi(R_o, \theta) = M$$

$$\left.\frac{\partial \chi}{\partial n}\right|_{R_o,\,\theta} = 0$$

Figure (A1c)

In this case σ_M is required to be zero and therefore $(\sigma_P + \sigma_M) = \sigma_P = P/B(W - a)$. This was accomplished by superposition of boundary conditions for the forces P, fig. (A1a) with those for countercouples of moment $P(R_i + (W + a)/2)$, fig. (A1b).

Figure (A1d)

For the pin loaded ring segment the boundary conditions of figs. (A1c) and (A1b) were superimposed. Here $M_{II} = P(x + (W + a)/2)$.

The boundary conditions for the externally cracked model are as follows:

Figure (A2a)

For the ring segment subjected to forces P, acting towards one another, with $\theta = \theta_o$ and boundaries AB, BC, CD: along arc AB

$$\chi(R_o, \theta) = 0$$

$$\left.\frac{\partial \chi}{\partial n}\right|_{R_o,\,\theta} = 0$$

along line BC

$$\chi(R, \theta_o) = \frac{P \cos \theta_o}{\left(R_i^2 - R_o^2\right) + \left(R_i^2 + R_o^2\right) \ln\left(\frac{R_o}{R_i}\right)}$$

$$\times \left[\frac{R^3}{3} - \frac{R_i^2 R_o^2}{2R} - R\left(\left(R_i^2 + R_o^2\right) \ln\left(\frac{R}{R_o}\right) + \frac{R_o^2 - R_i^2}{2}\right)\right]$$

$$\left.\frac{\partial \chi}{\partial n}\right|_{R, \theta_o} = \frac{-P \sin \theta_o}{\left(R_i^2 - R_o^2\right) + \left(R_i^2 + R_o^2\right) \ln\left(\frac{R_o}{R_i}\right)}$$

$$\times \left[\frac{R^2}{2} - \frac{R_i^2 R_o^2}{2R^2} - \left(R_i^2 + R_o^2\right) \ln\left(\frac{R}{R_o}\right) - \left(\frac{R_o^2 - R_i^2}{2}\right)\right]$$

along arc CD

$$\chi(R_i, \theta) = P R_i \cos \theta$$

$$\left.\frac{\partial \chi}{\partial n}\right|_{R_i, \theta} = -P \cos \theta$$

Figure (A2b)

For the couple load with $\theta = \theta_o$ and boundaries AB, BC, CD:

along arc AB

$$\chi(R_o, \theta) = 0$$

$$\left.\frac{\partial \chi}{\partial n}\right|_{R_o, \theta} = 0$$

along line BC

$$\chi(R, \theta_o) = \frac{-M}{\left(R_o^2 - R_i^2\right) - 4R_o^2R_i^2\left(\ln\frac{R_o}{R_i}\right)^2}$$

$$\times\left[-4\,R_i^2R_o^2\ln\frac{R_o}{R_i}\ln R - \left(2\,R_o^2 - R_i^2\right)R^2\ln R + R^2\left(R_o^2 - R_i^2\right)\right.$$

$$\left. + 2\left(R_o^2\ln R_o - R_i^2\ln R_i\right)R^2 + R_o^2\left(2\,R_i^2\ln\frac{R_o}{R_i}\left(2\ln R_o - 1\right) - \left(R_o^2 - R_i^2\right.\right.\right.$$

$$\left.\frac{\partial\chi}{\partial n}\right|_{R,\,\theta_o} = 0$$

along arc CD

$$\chi(R_i, \theta) = M$$

$$\left.\frac{\partial\chi}{\partial n}\right|_{R_i,\,\theta} = 0$$

Figure (A2c)

In this case σ_M is required to be zero and the loading forces act towards one another since the crack is external. It was treated by superposition of the boundary conditions of figs. (A2a) and (A2b), so that $(\sigma_P + \sigma_M) = \sigma_P = P/B(W - a)$ and the counter couple moment $M_I = P(R_i + (W - a)/2)$.

Figure (A2d)

This case of a pin loaded ring segment was treated by superposition of the boundary conditions of fig. (A2c) with (A2b), so that $M_{II} = P(x + (W - a)/2)$.

As discussed in ref. 6, the forms of the dimensionless coefficients

$$\Gamma = K_I/(\sigma_P + \sigma_M)\sqrt{a(1 - a/W)}$$

and

$$\Delta = E'v/(\sigma_P + \sigma_M)a$$

are particularly suitable for interpolation of combined cases (niether σ_P nor $\sigma_M = 0$) from the two complementary cases: (1) Γ_P and Δ_P, where $\sigma_M = 0$, tables I and IV; (2) Γ_M and Δ_M, where $\sigma_P = 0$, tables II and V. The fictitious stresses σ_P and σ_M are merely convenient functions of the first and second order moments P and M, of the distributions of internal normal forces acting on the net section in the plane of the crack: $\sigma_P = P/B(W - a)$ and $\sigma_M = 6\ M/B(W - a)^2$.

REFERENCES

1. 1974 Annual Book of ASTM Standards. Part 10 - Metals - Mechanical, Fracture, and Corrosion Testing; Fatigue; Crosion; Effect of Temperature, Am. Soc. for Testing and Materials (1974), 432-451.
2. D. P. Kendall and M. A. Hussain, Experimental Mech., 12 (1972) 184-189.
3. M. A. Hussain, et al., Watervliet Arsenal Rept. R-WV-T-X-6-73 (1973).
4. J. H. Underwood, R. D. Scanlon, and D. P. Kendall, Watervliet Arsenal Rept. R-WV-T-6-15-73 (1973).
5. Underwood, J. H. and Kendall, D. P.: K-Results and Comparisons For a Proposed Standard C-Specimen. In House Report (to be published), June 1974, Watervliet, N. Y.
6. J. E. Srawley and B. Gross, Side Cracked Plates Subject to Combined Direct and Bending Forces, presented at Ninth Symposium on Fracture Mechanics, Pittsburgh, Pa. (1975).
7. Y. C. Fung, Foundations of Solid Mechanics, Prentice-Hall Inc. (1965).
8. B. Gross, Ph.D. Thesis, Case Western Reserve Univ. (1970).
9. B. Gross and A. Mendelson, NASA TN D-6040 (1970).

TABLE I. - VALUES OF THE DIMENSIONLESS STRESS INTENSITY COEFFICIENT Γ_P FOR EDGE CRACKED RING SEGMENTS SUBJECT TO NET SECTION TENSION ($\sigma_M = 0$)

a/W	Internal crack			Straight* bar	External crack		
	R_o/R_i						
	2.5	1.5	1.1	1.0	1.1	1.5	2.5
	$\Gamma_P \frac{R_o}{R_i}, \alpha, \omega = \frac{K_I}{(\sigma_P + \sigma_M)\sqrt{a(1 - a/W)}}$						
0				1.989			
.1	1.527	1.474	1.463	1.466	1.476	1.492	1.549
.2	1.032	1.101	1.151	1.164	1.181	1.231	1.322
.3	.804	.882	.943	.961	.981	1.045	1.149
.4	.692	.752	.804	.822	.841	.904	1.010
.5	.636	.673	.711	.725	.740	.794	.892
.6	.604	.625	.650	.659	.669	.710	.791
.7	.583	.594	.608	.613	.620	.645	.704
.8	.564	.570	.577	.580	.582	.592	.629
1.0				.521			

*Ref. 6.

TABLE II. - VALUES OF THE DIMENSIONLESS STRESS INTENSITY COEFFICIENT Γ_M FOR EDGE CRACKED RING SEGMENTS SUBJECT TO NET SECTION BENDING ($\sigma_P = 0$)

a/W	Internal crack			Straight* bar	External crack		
	R_o/R_i						
	2.5	1.5	1.1	1.0	1.1	1.5	2.5
	$\Gamma_M(R_o/R_i, a/W, \omega) = \frac{K_I}{(\sigma_P + \sigma_M)\sqrt{a(1 - a/W)}}$						
0				1.989			
.1	1.943	1.736	1.623	1.583	1.552	1.456	1.325
.2	1.530	1.427	1.359	1.339	1.319	1.254	1.160
.3	1.279	1.221	1.182	1.167	1.155	1.110	1.040
.4	1.107	1.074	1.048	1.038	1.029	.997	.947
.5	.983	.963	.943	.938	.931	.911	.871
.6	.887	.872	.862	.858	.854	.839	.809
.7	.811	.803	.795	.794	.789	.780	.759
.8	.752	.747	.742	.742	.738	.732	.716
1.0				.663			

*Ref. 6.

TABLE III. - VALUES OF THE DIMENSIONLESS STRESS INTENSITY COEFFICIENT Γ FOR EDGE CRACKED RING SEGMENTS SUBJECT TO FORCES P ALONG THE

$$\left(\omega = \arctan\left(\frac{\frac{6}{(R_o/R_i - 1)} + 3 + 3\,a/W}{(1 - a/W)}\right)\right.$$ internal crack, and

$$\omega = \arctan -\left(\frac{\frac{6}{(R_o/R_i - 1)} + 3 - 3\,a/W}{(1 - a/W)}\right)\left.\right)$$ external crack

a/W	Internal crack			Straight* bar	External crack		
	2.5	1.5	1.1	1.0	1.1	1.5	2.5
	$\Gamma(R_o/R_i,\ a/W,\ \omega) = \frac{K_I}{(\sigma_M + \sigma_P)\sqrt{a(1 - a/W)}}$						
				1.989			
.1	1.897	1.721	1.623	1.583	1.555	1.456	1.290
.2	1.484	1.414	1.359	1.339	1.321	1.254	1.139
.3	1.241	1.210	1.180	1.167	1.154	1.111	1.024
.4	1.078	1.062	1.046	1.038	1.031	1.003	.938
.5	.963	.953	.943	.938	.933	.915	.868
.6	.873	.866	.862	.858	.856	.842	.810
.7	.803	.801	.795	.794	.791	.784	.761
.8	.747	.745	.742	.742	.740	.734	.721
1.0				.663			

*Ref. 6.

TABLE IV. - VALUES OF THE DIMENSIONLESS CRACK MOUTH DISPLACEMENTS, Δ_P, FOR EDGE CRACKED RING SEGMENTS SUBJECT TO NET SECTION TENSION ($\sigma_M = 0$)

a/W	Internal crack			Straight* bar	External crack		
	R_o/R_i						
	2.5	1.5	1.1	1.0	1.1	1.5	2.5
	$\Delta_P(R_o/R_i, a/W, \omega) = \frac{E'v}{(\sigma_P + \sigma_M)a}$						
0				5.84			
.1	4.28	4.01	3.60	3.69	3.69	3.81	4.12
.2	2.53	2.49	2.63	2.73	2.78	2.99	3.35
.3	1.32	1.53	1.75	1.85	1.91	2.17	2.60
.4	.378	.695	.963	1.06	1.14	1.44	1.94
.5	-.414	-.057	-.236	.331	.432	.762	1.31
.6	-1.10	-.745	-.453	-.357	-.254	.093	.677
.7	-1.72	-1.40	-1.11	-1.04	-.936	-.596	-.001
.8	-2.32	-2.04	-1.81	-1.73	-1.65	-1.36	-.800
1.0				-3.26			

*Ref. 6.

TABLE V. - VALUES OF THE DIMENSIONLESS CRACK MOUTH DISPLACEMENT, Δ_M, FOR EDGE CRACKED RING SEGMENTS SUBJECT TO NET SECTION BENDING ($\sigma_P = 0$)

a/W	Internal crack			Straight* bar	External crack		
	R_o/R_i						
	2.5	1.5	1.1	1.0	1.1	1.5	2.5
	$\Delta_M(R_o/R_i, a/W, \omega) = \frac{E'v}{(\sigma_P + \sigma_M)a}$						
0				5.84			
.1	5.47	4.81	4.51	4.40	4.28	4.05	3.81
.2	4.65	4.23	3.95	3.96	3.86	3.76	3.50
.3	4.14	3.84	3.63	3.67	3.57	3.43	3.21
.4	3.78	3.56	3.38	3.38	3.35	3.20	2.99
.5	3.51	3.33	3.20	3.18	3.14	3.02	2.83
.6	3.29	3.15	3.05	3.03	3.00	2.89	2.71
.7	3.11	3.00	2.94	2.90	2.87	2.79	2.64
.8	2.93	2.87	2.82	2.80	2.78	2.71	2.58
1.0				2.64			

*Ref. 6.

TABLE VI. - VALUES OF THE DIMENSIONLESS CRACK MOUTH DISPLACEMENT Δ, FOR EDGE CRACKED RING SEGMENTS SUBJECT TO OPPOSED FORCES P ALONG THE DIAMETER NORMAL TO THE CRACK PLANE

$$\left(\omega = \arctan\left(\frac{\frac{6}{(R_o/R_i - 1)} + 3 + 3\,a/W}{1 - a/W}\right)\right. \text{ internal crack,}$$

$$\omega = \arctan -\left(\frac{\frac{6}{(R_o/R_i - 1)} + 3 - 3\,a/W}{1 - a/W}\right)\left. \text{ external crack}\right)$$

a/W	Internal crack			Straight* bar	External crack		
	R_o/R_i						
	2.5	1.5	1.1	1.0	1.1	1.5	2.5
	$\Delta(R_o/R_i, a/W, \omega) = \frac{E'v}{(\sigma_P + \sigma_M)a}$						
0				5.84			
.1	5.31	4.73	4.45	4.40	4.22	3.66	2.87
.2	4.45	4.13	3.93	3.96	3.80	3.41	2.74
.3	3.90	3.75	3.61	3.67	3.50	3.16	2.59
.4	3.54	3.46	3.37	3.38	3.27	3.00	2.51
.5	3.28	3.24	3.18	3.18	3.11	2.88	2.48
.6	3.10	3.06	3.03	3.03	2.98	2.80	2.47
.7	2.95	2.93	2.90	2.90	2.86	2.74	2.46
.8	2.82	2.81	2.80	2.80	2.77	2.68	2.51
1.0				2.64			

*Ref. 6.

E-8567

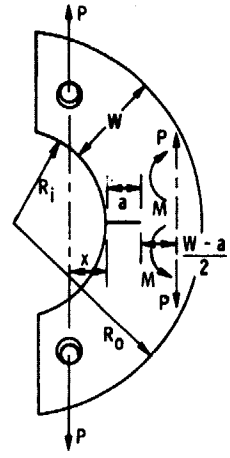

(a) INTERNAL RADIALLY CRACKED BAR WITH APPLIED LOAD P AT x.

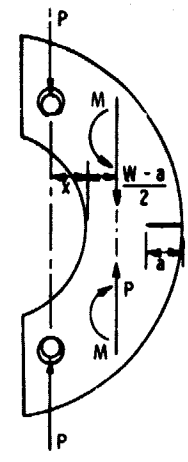

(b) EXTERNAL RADIALLY CRACKED BAR WITH APPLIED LOAD P AT x.

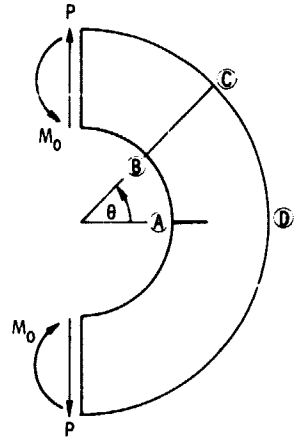

(c) INTERNAL RADIALLY CRACKED BAR WITH APPLIED LOADS P AND M_o AT $x = R_i$.

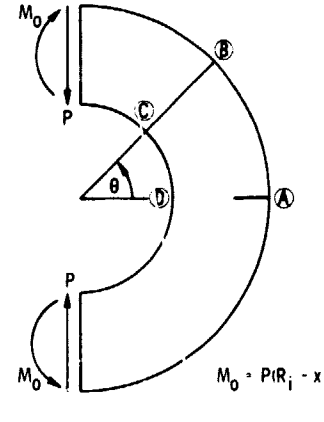

(d) EXTERNAL RADIALLY CRACKED BAR WITH APPLIED LOADS P AND M_o AT $x = R_i$.

Figure 1. - Ring segment models.

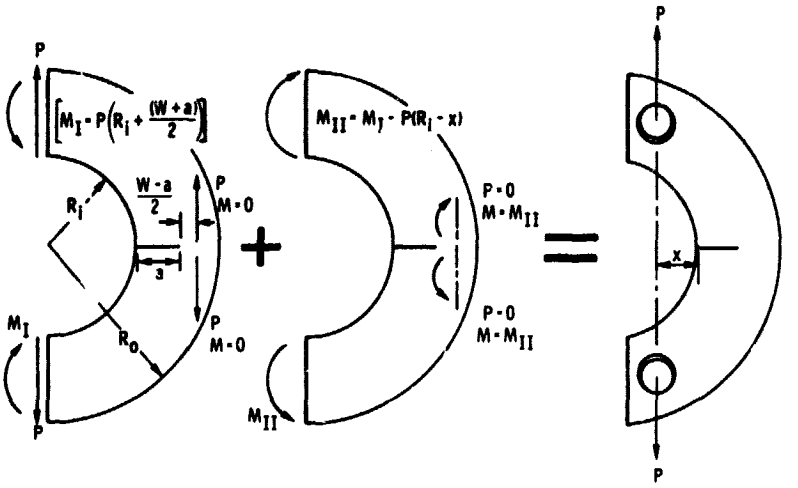

Figure 2. - Application of superposition to specimen loaded through pins at selected distance x from crack mouth.

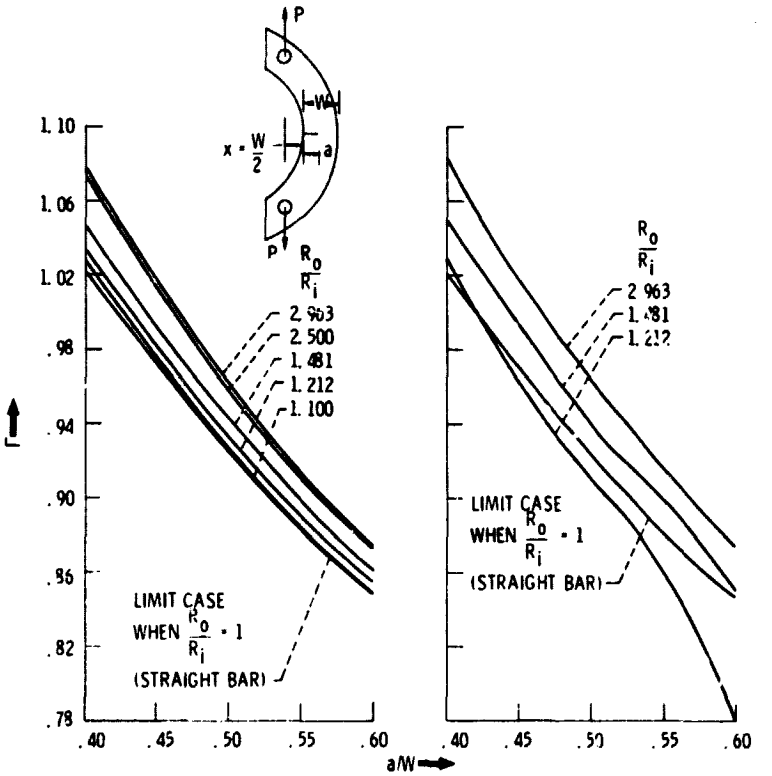

(a) RESULTS OF THIS STUDY. (b) RESULTS OF REFERENCE 5.

Figure 3. - Comparison of results obtained herein with those reference 5 for x/W = 0.5.

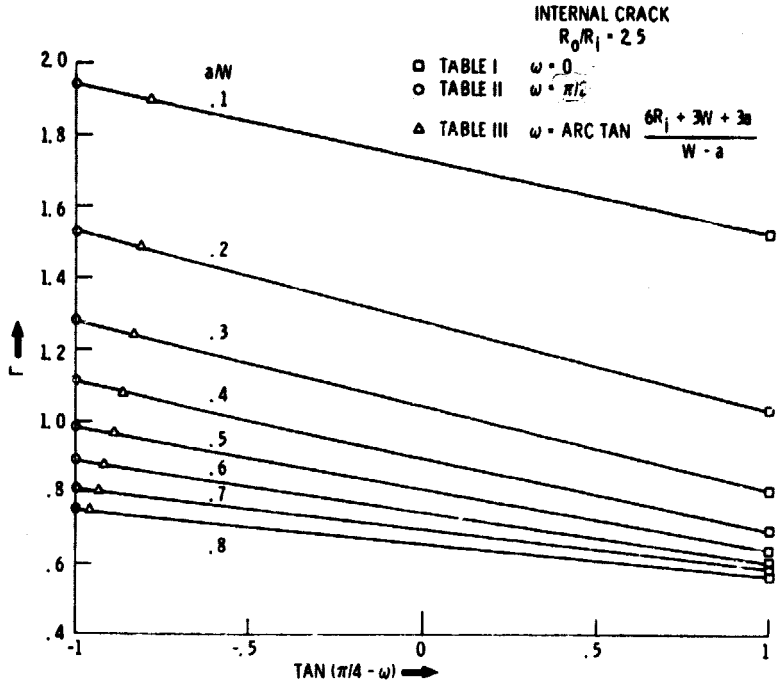

Figure 4. - Γ vs tan ($\pi/4 - \omega$) illustrating the advantage using tables I and II for superposition application, rather than tables II and III.

E-8567

$\frac{R_o}{R_i}$	θ_o	$\frac{H_i}{R_o - R_i}$	$\frac{H_o}{R_o - R_i}$
1.1	7°	1.22	1.34
1.5	30°	1.00	1.5
2.5	40°	.43	1.07

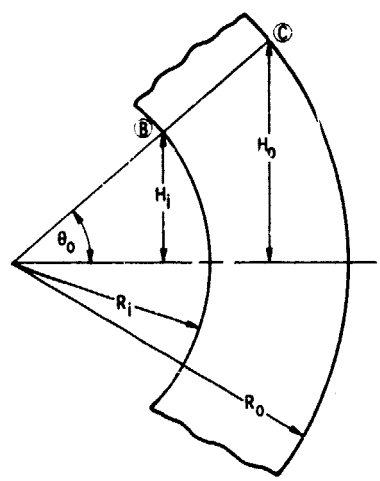

Figure 5. - Minimum location of far boundary Ⓑ Ⓒ for which the stress distribution in an uncracked ring corresponds to that used herein.

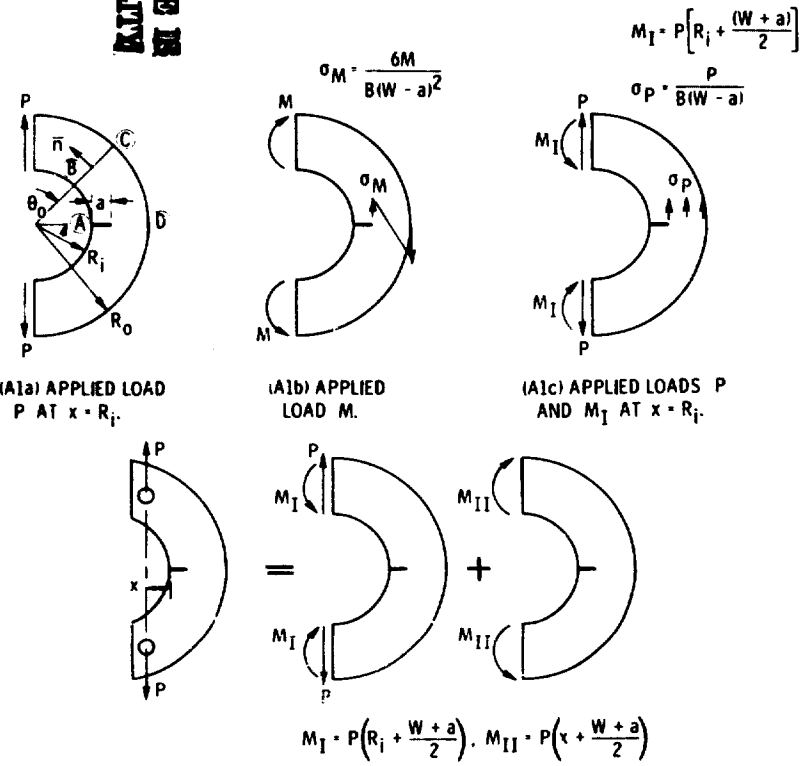

(A1a) APPLIED LOAD P AT $x = R_i$.

(A1b) APPLIED LOAD M.

(A1c) APPLIED LOADS P AND M_I AT $x = R_i$.

(A1d) APPLICATION OF SUPERPOSITION PRINCIPLE.

Figure A1. - Geometric models used for the internal radially cracked ring segment to obtain the necessary boundary conditions for the application of the superposition principle.

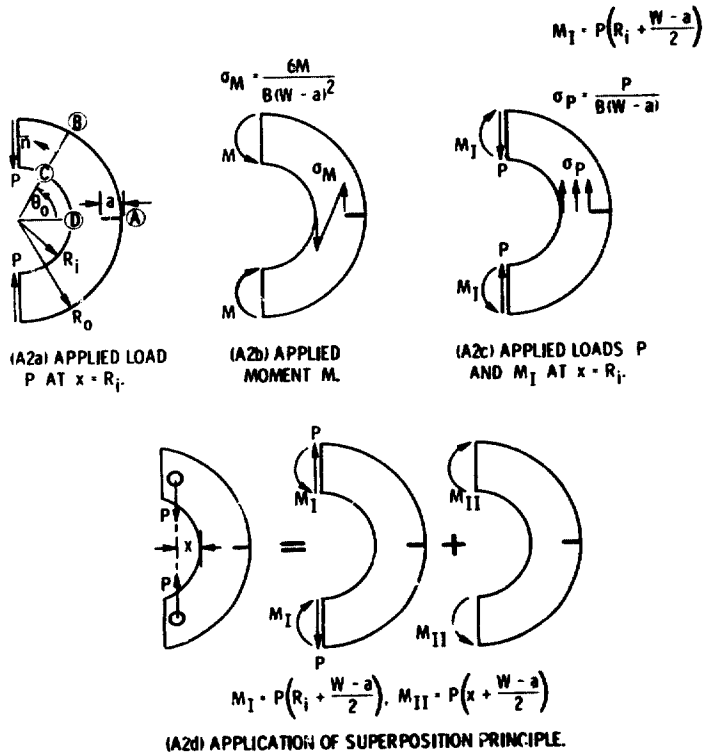

(A2a) APPLIED LOAD P AT $x = R_i$.

(A2b) APPLIED MOMENT M.

(A2c) APPLIED LOADS P AND M_I AT $x = R_i$.

(A2d) APPLICATION OF SUPERPOSITION PRINCIPLE.

Figure A2. - Geometric models used for the external radially cracked ring segment to obtain the necessary boundary conditions for the application of the superposition principle.